KSME

Springer

Journal of Mechanical Science and Technology 36 (3) 2022

Original Article
DOI 10.1007/s12206-022-0230-7

Keywords:
· Composite conical shell
· Equidistant offset surface
· Path planning
· Fiber placement

Correspondence to:
Jun Hu
hjmorning@hotmail.com;
Kangmei Li
lkm718@126.com

Citation:
Xu, H., Lu, J., Li, K., Hu, J. (2022). Design and analysis of fiber placement for composite conical shell. Journal of Mechanical Science and Technology 36 (3) (2022) 1427~1436.
http://doi.org/10.1007/s12206-022-0230-7

Received July 1st, 2021
Revised November 15th, 2021
Accepted November 30th, 2021

† Recommended by Editor Hyung Wook Park

Design and analysis of fiber placement for composite conical shell

Haojie Xu[1], Jiuru Lu[1], Kangmei Li[2,3] and Jun Hu[4]

[1]College of Mechanical Engineering, Donghua University, Shanghai 201620, China, [2]Shanghai Collaborative Innovation Center for High Performance Fibercomposites, College of Mechanical Engineering, Donghua University, Shanghai 201620, China, [3]State Key Lab of Digital Manufacturing Equipment & Technology, Wuhan, Hubei 430074, China, [4]Institute of Artificial Intelligence, Donghua University, Shanghai 201620, China

Abstract Composite conical shells have a wide range of applications. The 3D printing technology based on FDM constrains the fibers in a plane and it is difficult to fill the fibers in the thin wall. This paper proposes a rapid prototyping method for composite materials based on curved surface fiber placement. The conical shell is divided into a series of equidistant offset surfaces. Then we designed three initial paths for fiber placement and rotated them to cover the surface of the conical shell. The resin paths are designed for filling the border layers and the gaps between the fibers. The placement process is simulated by MATLAB (R2016b) and we analyzed the parameter range, direction angle, curvature and fiber content of the three paths. When the critical parameters φ_0 = [0°, 42°], ξ is equal to any value and C = (0, 0.032], the corresponding initial path can reach the top of the cone shell in this study. The direction of the constant curvature curve can be designed best; when C = 0.032, the direction angle range is -90 to 90. The curvature of the geodesic path is the smallest; when φ_0 = 10°, the normal curvature is about 0.0001 and the geodesic curvature is equal to 0. The fiber content of the geodesic path is greatly affected by the parameter φ_0, and the difference can reach 40 %. The fiber content of the linear curve is greater than 90 %. When ξ is equal to 4, the fiber content is 95 %. For the constant curvature curve, the fiber content is generally very low, about 20 %. We used a six-axis robot and a spindle to produce composite conical shell. The results show that the present design method for composite conical shell is reliable and is able to provide a useful reference for design and production of composite conical shell.

1. Introduction

Composite material is prepared with fiber as the reinforcement and resin as the matrix. Composites are applied in aerospace and automobile industries because of high specific strength and high specific modulus. For example, composite conical shells are often used in rocket exhaust cones, diffusion sections and fairings. At present, the common manufacturing processes of composite material include molding pressing, filament winding (FW), automated tape laying (ATL), and automatic fiber placement (AFP). These conventional processes cannot freely design fiber paths while ensuring the surface quality of the parts [1].

Fused deposition modeling (FDM) is one of the most commonly used 3D printing technologies for manufacturing composite materials. It provides a method that can freely change the placement direction of fiber for the manufacture of composite material, so as to realize the designability of structural performance [2-5]. At present, the FDM-based composite 3D printing technology uses the plane slicing method to layer the 3D digital model, and then design the fiber path layer by layer. In 2014, Mark forged developed a dual-nozzle composite 3D printer [6]. Arevo Labs launched the robotic arm 3D printing platform RAM in 2015, which can be used to print high-performance carbon fiber reinforced thermoplastic composite parts [7]. Envision TEC developed the SLCOM1 3D printer, which can realize the industrial production of carbon fiber fabrics and composite materials, and can be applied to a variety of thermoplastic resin systems [8]. Tian et

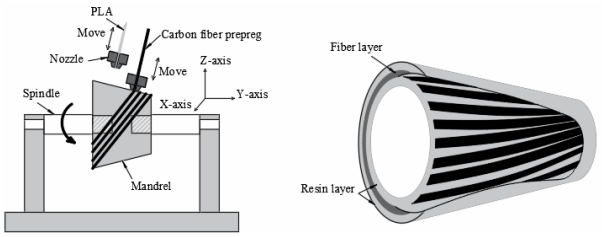

Fig. 1. (a) Production equipment; (b) composite conical shell.

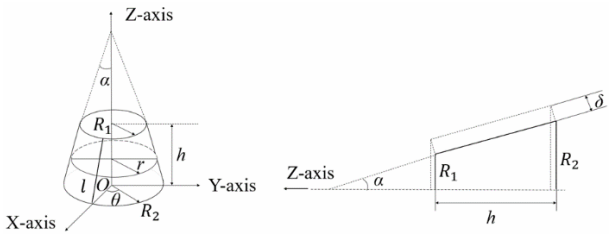

Fig. 2. (a) Conical shell geometry model; (b) offset surface.

al. manufactured CFRTPCs components through a 3D printing process; interfaces and performance of printed composites were systematically studied by analyzing the influencing of process parameters on the temperature and pressure in the process [9]. Because the fibers are constrained in a plane, the use of this 3D printing process to produce a thin-walled cone shell makes the mechanical properties of the cone shell in the vertical direction poor. Furthermore, it is difficult or even impossible to fill fibers in thin walls, which results in a low fiber content here.

The main goal of this paper is to study a design and production method that fibers are placed on curved surface for composite conical shell with thin wall. We refer to the characteristics of curved fiber placement technology and 3D printing technology, and extend the 3D printing slicing principle from a flat surface to a curved surface. In a typical process, under the coordinated movement of the nozzle and the core mold, the heated and melted resin is deposited on the surface of the core mold through a nozzle, which is called as resin layer in this paper. The pre-prepared mixed material of fiber and resin is heated, and then placed on the resin layer through another nozzle. The fiber is placed layer by layer on the curved surface. Finally, the curved surface is covered with melted resin again, and a designed thin-walled cone shell is formed as shown in Fig. 1.

In this work, we studied the mathematical model of the conical shell offset surface. Then, three fiber initial paths were derived, which are rotated to cover the conical shell surface. The resin paths are designed for filling the border layers and the gaps between the fibers. We simulated the placement process with MATLAB (R2016b) and analyzed the parameter range, direction angle, curvature and fiber content of the three paths. We used a six-axis robot and a spindle to produce composite conical shell. The results show that the method is able to provide a useful reference for the design and production of composite conical shell.

2. Mathematical model

2.1 Offset surface

In the process of fiber placement and resin filling, the surface of the conical shell becomes thicker layer by layer. If the mathematical model of the conical shell were not changed, the accuracy of the molded part would be affected [10]. Therefore, we first discuss the offset of the conical shell surface. As shown in Fig. 2(a), the semi apex angle α of a conical shell with small end radius R_1, large end radius R_2, and height h can be expressed as:

$$\tan\alpha = \frac{R_2 - R_1}{h}. \tag{1}$$

For a conical shell, the radius of any axial section is a linear function of z:

$$r(z) = -z \cdot \tan\alpha + R_2. \tag{2}$$

The conical shell can be expressed as a curved surface swept by a generatrix l rotating counterclockwise around the Z axis, where the origin O of the cartesian coordinate system is located at the center of the large end section of the cone. At this time, the surface of the conical shell can be expressed in a cylindrical coordinate system {r, θ, z}:

$$\mathbf{r}(\theta, z) = (r \cdot \cos\theta, r \cdot \sin\theta, z) \tag{3}$$

where $r = r(z)$, θ is the center angle. For the unit normal vector of any point P on the conical shell surface **r** (θ, z) is:

$$\boldsymbol{n} = \frac{\mathbf{r}_\theta \times \mathbf{r}_z}{|\mathbf{r}_\theta \times \mathbf{r}_z|} = \left(1 + r'^2\right)^{-\frac{1}{2}} (\cos\theta, \sin\theta, -r'). \tag{4}$$

As shown in Fig. 2(b), we offset each point on the surface of the conical shell by a certain distance δ along the normal vector to obtain the offset surface of the conical shell:

$$\mathbf{r}_i(\theta, z) = \mathbf{r}(\theta, z) + \delta_i \cdot \boldsymbol{n}. \tag{5}$$

2.2 Initial paths of fiber

As shown in Fig. 3, P is a point on the curve, ***n*** is the normal vector of the surface at that point, and $\boldsymbol{\tau}$ is the tangent vector of the surface at that point along the direction of the curve.

The coefficients of the first fundamental form and the second

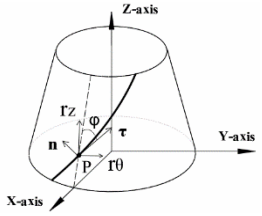

Fig. 3. Vectors of the conical shell.

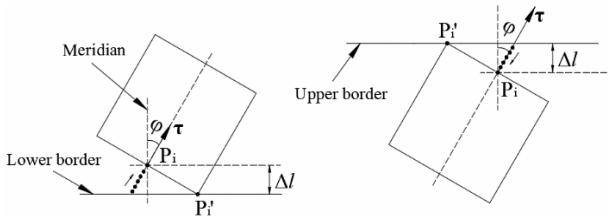

(a) (b)

Fig. 4. (a) Conical shell lower border; (b) conical shell upper border.

fundamental form of r(θ, z) are:

$$\begin{cases} E = r_\theta \cdot r_\theta = r^2 \\ F = r_\theta \cdot r_z = 0 \\ G = r_z \cdot r_z = 1 + r'^2 \end{cases} \quad \begin{cases} L = r_{\theta\theta} \cdot \mathbf{n} = -r\left(1 + r'^2\right)^{-1/2} \\ M = r_{\theta z} \cdot \mathbf{n} = 0 \\ N = r_{zz} \cdot \mathbf{n} = r''\left(1 + r'^2\right)^{-1/2} \end{cases} . \tag{6}$$

Substituting Eq. (6) into the first fundamental form of r(θ, z), the differential terms dθ/ds and dz/ds can be given by:

$$\frac{d\theta}{ds} = \left(\frac{r^2\theta'^2 + 1 + r'^2}{\theta'^2}\right)^{-1/2}, \frac{dz}{ds} = (r^2\theta'^2 + 1 + r'^2)^{-1/2} \tag{7}$$

where *s* is the length of the curve. The tangent vector of the curve on r(θ, z) can be expressed as:

$$\boldsymbol{\tau} = \mathbf{r}_\theta \frac{d\theta}{ds} + \mathbf{r}_z \frac{dz}{ds} . \tag{8}$$

The fiber direction angle φ which is the angle between the curve tangent and the meridian can be given by:

$$\cos\varphi = \frac{\boldsymbol{\tau} \cdot \mathbf{r}_z}{|\boldsymbol{\tau}| \cdot |\mathbf{r}_z|} = \left(\frac{1 + r'^2}{r^2\theta'^2 + 1 + r'^2}\right)^{1/2} \tag{9}$$

where θ' = dθ/dz. According to Eq. (9), the expression of θ' can be given by:

$$\theta' = \frac{1}{r}\left(1 + r'^2\right)^{1/2} \tan\varphi . \tag{10}$$

Combining the first basic form and the second basic form of the surface r(θ, z), we can get the normal curvature of the surface:

$$k_n = \frac{\text{II}}{\text{I}} = \frac{L \cdot (d\theta)^2 + 2M \cdot d\theta dz + N \cdot (dz)^2}{E \cdot (d\theta)^2 + 2F \cdot d\theta dz + G \cdot (dz)^2} = \frac{r\theta'^2 - r''}{(1 + r'^2)^{1/2}(r^2\theta'^2 + 1 + r'^2)} . \tag{11}$$

According to the general formula of geodesic curvature, the geodesic curvature can be given by:

$$k_g = \boldsymbol{\tau}' \cdot (\boldsymbol{n} \times \boldsymbol{\tau}) = \frac{(1 + r'^2)(2r'\theta' + r\theta'') + rr'\theta'(r\theta'^2 - r'')}{(1 + r'^2)^{1/2}(1 + r'^2 + r^2\theta'^2)^{3/2}} \tag{12}$$

where $\boldsymbol{\tau}'$ = $\boldsymbol{\tau}$' (s), r' = r' (z), r'' = r'' (z).

In this study, the following three different fiber paths are considered [11].

1) Linear curve:

$$\theta(z) = \xi \cdot \pi \cdot \frac{z}{h} \tag{13}$$

where ξ is the coefficient of the linear curve.

2) Geodesic path:

When kg = 0 in Eq. (12), the integration of both ends of the equation is the law of geodesic winding:

$$\theta'' = -\frac{rr'\theta'(r\theta'^2 - r'') + 2r'\theta'(1 + r'^2)}{r(1 + r'^2)} . \tag{14}$$

3) Constant curvature curve:

When kg = C in Eq. (12), combining the initial value of the first-order differential equation obtained by Eq. (10), solve Eq. (14) to obtain the corresponding values of z and θ:

$$\theta'' = \frac{C \cdot (1 + r'^2)^{1/2}(1 + r'^2 + r^2\theta'^2)^{3/2} - rr'\theta'(r\theta'^2 - r'') - 2r'\theta'(1 + r'^2)}{r(1 + r'^2)} . \tag{15}$$

Any arc on the flattened cone is a curve with equal geodesic curvature in space [12]. Therefore, we can find the arc of curvature equal to C in the flattened cone, which is the curve of kg = C in space.

As shown in the Fig. 4, at both ends of the initial path, the borders of the fiber at point P_i are just at the critical position where all the fibers fall on the surface of the conical shell. Therefore, we need to filter the points at both ends of the initial path to ensure that the fiber does not exceed the border of the conical shell. The distance between point P_i on the initial path and the corresponding point P_i' on the fiber border in the meridian direction can be approximately expressed as:

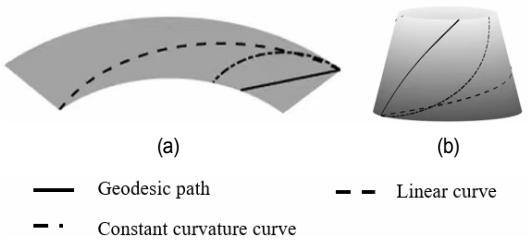

Fig. 5. Initial path: (a) flattened cone; (b) cone geometry.

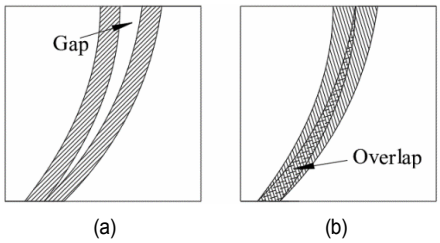

Fig. 6. Gap and overlap.

$$\Delta l = \frac{w_1 \sin\varphi}{2}. \tag{16}$$

If this distance is less than the distance of point P_i from the border of the cone in the meridian direction, it can be considered that the fiber falls on the surface of the cone at this point. This method redefines the starting point and end point of the initial path. At the same time, it can also screen out the points with too large direction angles at both ends.

3. Placement simulation

3.1 Initial path simulation

To verify the feasibility of the paths, with the help of MATLAB, the geometric model of the conical shell is established in the cartesian coordinate system. Then the fiber placement and resin filling are simulated according to the three initial paths.

In this simulation, R_1 is 30 mm, R_2 is 45 mm and the height h is 60 mm. Carbon fiber width w_1 is 1 mm, resin width w_2 is 1.5 mm. The center of the constant curvature curve is on the meridian of the flattened cone. As shown in Fig. 5, we simulate the three initial paths in the conical shell and the flattened cone with MATLAB (φ_0 = 30°, $\xi = 2$, $C = 1.62\times10^{-2}$). φ_0 represents the direction angle of the geodesic path at the starting point.

3.2 Fiber covering

To cover the surface of the conical shell with the initial path, we can make the initial path rotate at equal angles around the Z axis, which will cause gaps and overlap, as shown in Fig. 6. The gaps and overlap of the fiber during the placement process will affect the uniformity of the thickness, thereby affecting the dimensional accuracy and mechanical properties [13]. This section solved the fiber overlap problem by restricting the rotation angle.

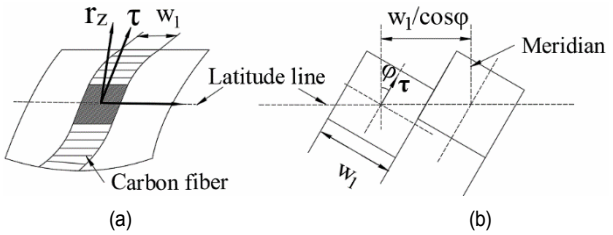

Fig. 7. (a) An element on fiber; (b) the limit position where fiber does not overlap.

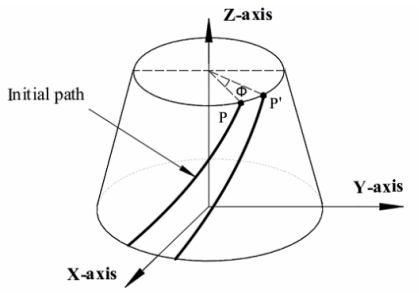

Fig. 8. The initial path rotates around the Z axis.

The specific steps for the initial path of the conical shell to cover the surface are as follows:

1) Determining the number of rotations of the initial path.

The number of rotations of the initial path is determined by the fiber width w_1 and z together. We take a small surface on the conical shell, as shown in Fig. 7, assuming that the fiber direction angle remains unchanged on the surface of the element, the number of rotations can be expressed as:

$$N_{\min} = \left\lfloor \frac{2\pi \cos\varphi_i r_i}{w_i} \right\rfloor. \tag{17}$$

2) Rotating the initial path around the Z axis.

As the number of rotations of the initial path is determined, the angle of each rotation can be expressed as:

$$\phi = \frac{2\pi}{N_{\min}}. \tag{18}$$

As shown in Fig. 8, there is a point P {x, y, z} on the curve C. The point P' {x', y', z'} after rotating ϕ around the Z axis can be expressed as:

$$P'\{x', y', z'\} = [x, y, z] \cdot R_z(\phi) \tag{19}$$

where Rz (ϕ) is the rotation matrix, it can be expressed as:

$$R_z(\phi) = \begin{bmatrix} \cos\phi & \sin\phi & 0 \\ -\sin\phi & \cos\phi & 0 \\ 0 & 0 & 1 \end{bmatrix}. \tag{20}$$

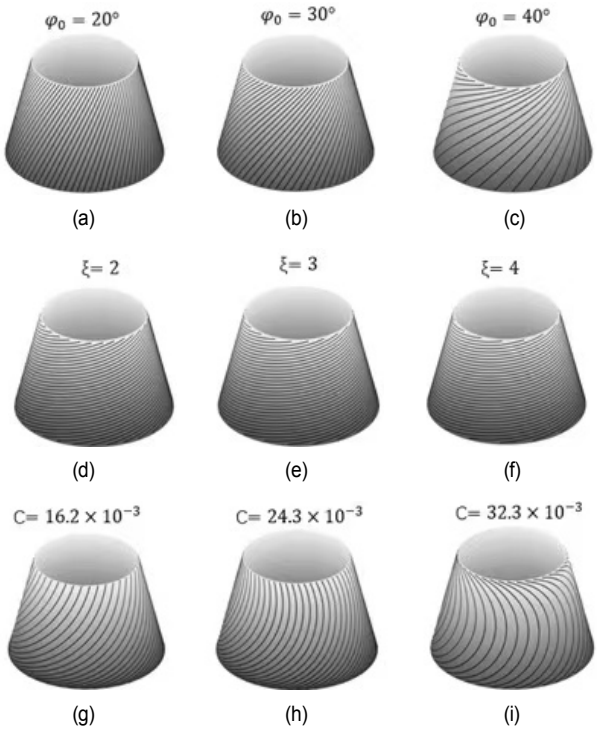

Fig. 9. Placement simulation in MATLAB: (a), (b), (c) geodesic path; (d), (e), (f) linear curve; (g), (h), (i) constant curvature curve.

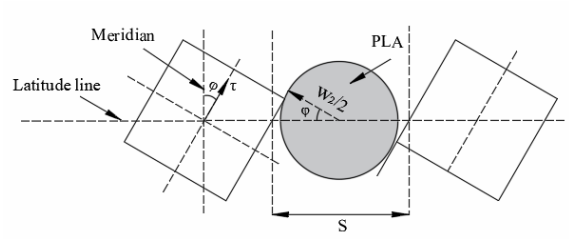

Fig. 10. The extreme position of resin filling.

As shown in Fig. 9, the conical shell surface can be covered with the initial path by constantly changing the value of ϕ.

3.3 Gap filling path

In the fiber initial path rotation algorithm we used, the rotation angle ϕ is the maximum angle to ensure that the fibers at each point on the initial path will not overlap. As the fiber direction angle and cross-sectional radius of the initial path are constantly changing, the circumferential distance between the fibers will increase, which creates gaps. This will affect the surface quality of the next layer of curved surface, resulting in uneven thickness. In this study, resin was used to fill the gaps between the fibers.

The resin filling can be regarded as a process in which a circle of diameter w_2 moves on a path. As shown in Fig. 10, we consider the extreme position where the resin can just start filling. At this time, distance of the gap in the circumferential direction can be expressed as:

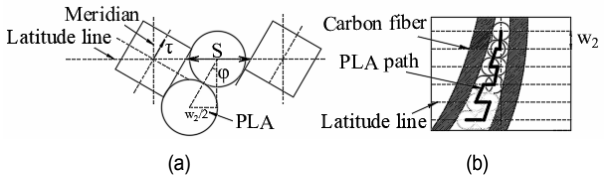

Fig. 11. (a) Limit filling position of adjacent layer; (b) resin filling path between gaps.

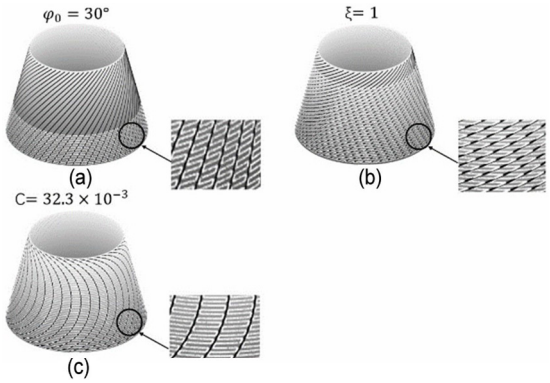

Fig. 12. Resin filling path simulation in MATLAB.

$$S = \frac{w_2}{\cos\varphi}. \tag{21}$$

Since the angle of rotation ϕ is determined, the corresponding z coordinate value according to Eq. (2) can be expressed as:

$$z_0 = \frac{R_2}{\tan\varphi} - \frac{360 w_2}{\sin\varphi\pi\phi}. \tag{22}$$

We divide the Z = [0, z0] equally in the axial direction as:

$$z_i = z_0 - i\cdot\Delta z, \quad \left(i = 1,2,...,\lfloor z_0/\Delta z \rfloor\right) \tag{23}$$

where $\triangle z = w_2 \cos\alpha$.

As shown in Fig. 11, at any position in the circumferential direction, we can take a circle with a diameter of $w_2/2$ at the extreme position on both sides of the gap. We use straight lines to connect the center of the circle in turn, which is the resin path.

As shown in Fig. 12, we simulate the results of resin filling between gaps in MATLAB. The black line represents the fiber path, and the white line the resin path. The results show that this method is feasible.

3.4 Border layer filling path

The innermost layer and the outermost layer of composite

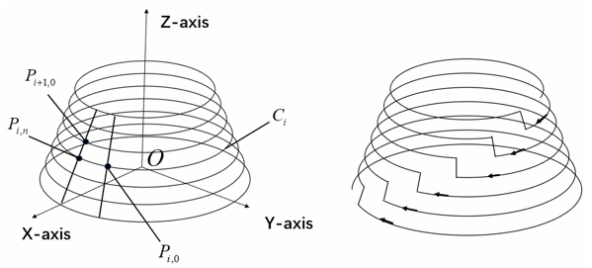

Fig. 13. (a) Discretizing the surface into a series of concentric circles; (b) spiral filling path.

conical shell need to be filled with resin to wrap the fibers. A continuous and efficient path should be considered to fill the border layers of the composite conical shell. Based on the principle of spiral offset in 3D printing, we used a resin filling method suitable for curved surfaces [14, 15]. First, the conical shell needs to be discrete into a series of concentric circles in space, as shown in the Fig. 13(a). To avoid overlap and gaps, the distance that the conical shell is equally divided along the Z axis can be expressed as:

$$\Delta z = w_2 \cdot \cos\alpha \,. \tag{24}$$

On curve C_i, we denote the starting point as $P_{i,0}$ and the ending point as $P_{i,n}$. To connect the two curves to make the trajectory continuous, the end point of C_i and the start point of C_{i+1} are located on the same meridian, and the length between $P_{i,0}$ and $P_{i,0}$ in C_i is w_2. Fig. 13(b) shows the resin filling path after using the spiral algorithm. The starting point $P_{i,0}$ of the curve C_i can be represented by {ρ, θ, z}:

$$P_{i,0}: \begin{cases} \rho = r(z_i) \\ \theta = \sum_{j=1}^{i-1} \dfrac{w_2 \cdot 180}{r(z_j)\cdot \pi}, (\theta_{1,0} = 0) \\ z = z_i \end{cases} . \tag{25}$$

4. Results and discussion

Four main results are reported. First, we analyzed the relationship between the three critical parameters and the maximum height of the path, and determined the range of the parameters. Second, we calculated the fiber direction angles at different heights when the three paths take different parameters according to Eq. (9). Third, considering the influence of path curvatures on fiber quality, we calculated the curvatures k_n and k_g in Fig. (17). Finally, we calculated the fiber content of different paths by calculating the ratio of the area of the fiber on the surface to the area of the surface in Figs. 18(d)-(f). We divided the cone shell into micro-elements along the height direction, and obtain the changing trend of fiber content and height under different paths in Figs. 18(a)-(c).

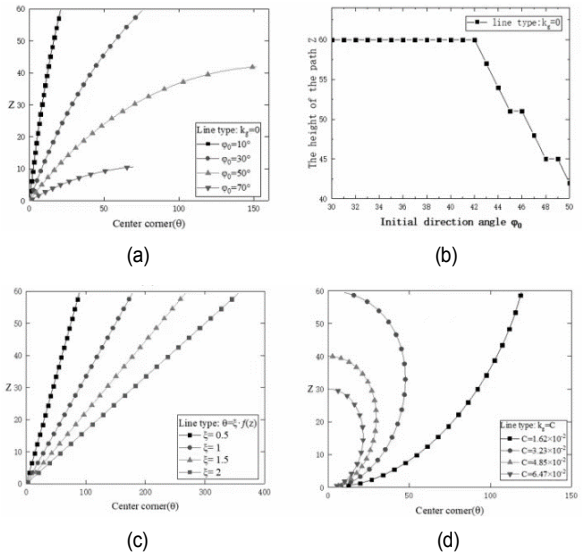

Fig. 14. The relationship between the parameters and the height of the fiber: (a) geodesic path; (b) critical parameter of the geodesic path; (c) linear curve; (d) constant curvature curve.

4.1 Critical parameters

Fiber plays an important role in enhancing the mechanical properties of composite materials. As the critical parameters of the initial path change, there will be cases where the fiber cannot reach the top of the cone (z = 60 mm). For the geodesic path, the critical parameter is the initial direction angle φ_0. It represents the direction angle of the fiber path at the starting point. For the linear curve, the critical parameter is the coefficient ξ. For the constant curvature curve, the critical parameter is the value of geodesic curvature C. The critical parameter will affect the maximum height of the path on the surface. Fig. 14 shows the relationship between each key parameter and the height of the path.

As shown in Figs. 14(a) and (b), when the initial direction angle φ_0 is equal to 43°, the maximum height of the geodesic path is 57 mm. Then as φ_0 increases, the height of the path gradually decreases. For a linear curve, shown in Fig. 14(c), it always can reach the top of the conical shell. Because the height z is a linear function of θ, for any value of ξ, there will always be a θ to make z = 60 mm. The maximum coefficient of the constant curvature curve that can reach the top of the cone is C = 0.032 in Fig. 14(d). At this time, the constant curvature curve in the flattened cone is an arc with a meridian as its diameter. Then as the value of C increases, the path cannot reach the top of the cone.

4.2 Direction angle

The mechanical performance of the composite materials is directly determined by the direction of the fiber [16, 17]. In a typical laminated composite plate, 0°, ±45°, and 90° are adopted as the layer orientations, which severely limits the

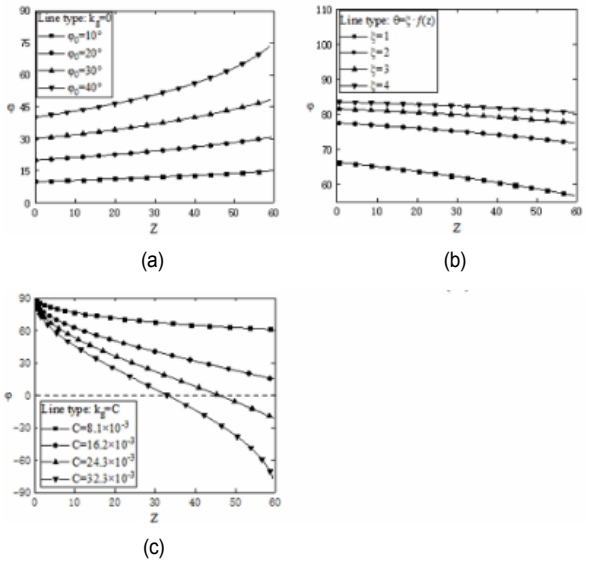

Fig. 15. Analysis of fiber direction angle: (a) geodesic path; (b) linear curve; (c) constant curvature curve.

designability of composite materials. The three fiber paths in this paper have different direction angles at different heights of the curved surface. We changed the critical parameters to get the direction angle change trend of different paths, and the results are shown in Fig. 15.

The strength of the composite material in the direction of fiber is relatively high. The analysis of the fiber angle can provide a reference for us to design the mechanical properties of the composite cone shell. It can be seen from Fig. 15(a) that within the parameter range, the maximum direction angle of the geodesic path φ is equal to 75°, which means that the fibers are mainly placed along the circumferential direction. In particular, when the initial direction angle φ_0 is equal to 0°, the geodesic path coincides with the meridian. At this time, the fiber direction is along the axial direction. Obviously, the range of the direction angle of the geodesic path is 0° to 72°. With the ξ value in Fig. 15(b), direction angles of linear curves are relatively large, almost all greater than 60°. However, the magnitude of the change is not large. When ξ is equal to 4, the difference in direction angle between the two ends is 4°. The fiber placement direction is mainly along the circumferential direction. However, through the analysis of Eq. (13), when the linear coefficient ξ is close to 0, the linear curve coincides with the meridian so the direction angle is equal to 0. For the constant curvature curve, when the parameter C takes the minimum value of 0.032, the fiber direction angle decreases from 90° to -90°. At this time, the variation range of the fiber direction angle is the largest, reaching 180°. As the parameter C decreases, the direction angle changes gradually. When C = 0.016, the fiber direction angles are all positive, as shown in Fig. 15(c).

4.3 Curvature

Generally, the fiber bundle has a strong ability to withstand deformation along the fiber direction, but weak ability to withstand transverse bending deformation. Due to the large elastic modulus of fiber prepreg, micro-buckling caused by compression causes fiber deformation, and the magnitude of strain is positively correlated with the geodesic curvature k_g [18].

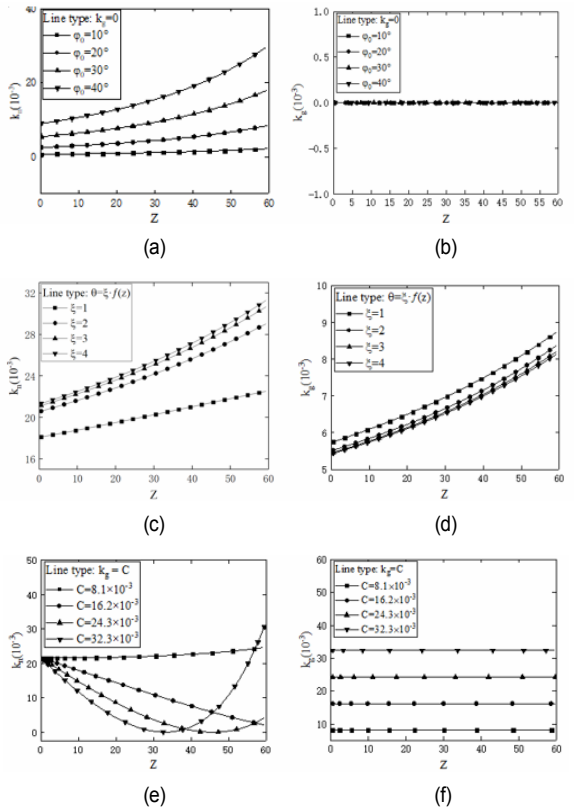

Fig. 16. Curvatures of the paths: (a) the k_n of the geodesic path; (b) the k_g of the geodesic path; (c) the k_n of the linear curve; (d) the k_g of the linear curve; (e) the k_n of the constant curvature curve; (f) the k_g of the constant curvature curve.

The normal curvature k_n is expressed in the degree of bending of the fiber in the thickness direction. According to Eqs. (11) and (12), we calculated the curvatures k_n and k_g of each point on the paths, as shown in Fig. 16.

It can be seen from Fig. 16(a) that within the parameter φ_0 range, the maximum curvature k_n of the geodesic path is equal to 0.027. When φ_0 is equal to 10°, the k_n of the points on the path are all close to 0. The reason is that as φ_0 approaches 0°, the geodesic path approaches the meridian. In Fig. 16(c), comparing the paths with parameter ξ = 3 and ξ = 4, the corresponding k_n differs by only 0.001. Because the two paths are similar at this time. According to the expression of the linear curve, we can also think that the maximum curvature k_n = 0.03 at this time is close to the maximum curvature that all linear curves can reach. Fig. 16(e) shows that for the constant curvature curve, when the geodesic curvature k_g is equal to the largest value (C = 0.032), the curvature k_n decreases from 0.021 to 0, and then increases to 0.03.

According to the definition of geodesic lines, the geodesic

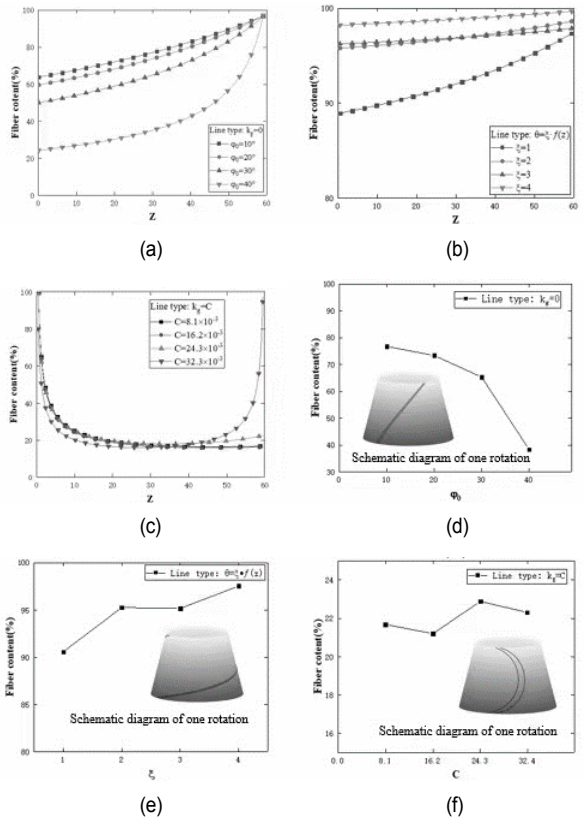

Fig. 17. Fiber content: (a) at different heights of the geodesic path; (b) at different heights of the linear curve; (c) at different heights of the constant curvature curve; (d) the geodesic path; (e) the linear curve; (f) the constant curvature curve.

curvature k_g of all geodesic lines is 0 in Fig. 16(b). This means that the fiber will not fold in the width direction when it is placed along the geodesic path. In Fig. 16(d), the curvature k_g of the linear curve is in a small range, and the maximum value is 0.0088. The curvature k_g of the constant curvature curve is determined by its parameter C, as shown in Fig. 16(f). Therefore, in this paper, the maximum curvature k_g of the constant curvature curve is 0.032.

4.4 Fiber content

Fiber content is an important indicator of composite materials. Generally, the mechanical strength of composite materials is directly proportional to the fiber content [19, 20]. In the carbon fiber placement process, the fibers are continuously distributed on a curved surface according to the designed path. Multiplying the length of the path by the width of the fiber, we can get the area of the fiber on the curved surface. To compare the coverage of different fiber paths on the curved surface, we regard the carbon fiber content as the ratio of the area of the carbon fiber on the curved surface to the area of the surface. By dividing the curved surface into micro-elements, Figs. 17(a)-(c) show the fiber content changes of the three fiber paths at different heights. The fiber content of the three paths is shown in Figs. 17(d)-(f).

For the conical shell placed with the geodesic line as the initial path, the maximum fiber content is 78 % in Fig. 17(d). When the initial direction angle φ_0 is 40°, the fiber content is only 38 %. The reduction reaches 51 %. As shown in Fig. 17(a), the reason is that the large rotation angle reduces the content of fiber where the radius of the cone is large at this time. When the linear curve is used as the initial path, the fiber content exceeds 90 % in Fig. 17(e). However, the fiber content of the conical shell with the constant curvature curve as the initial path is generally very low, about 20 % in Fig. 17(f), because the direction angle of some points is too large. Therefore, to avoid fiber stacking, a large rotation angle results in low fiber content, as shown in Fig. 17(c).

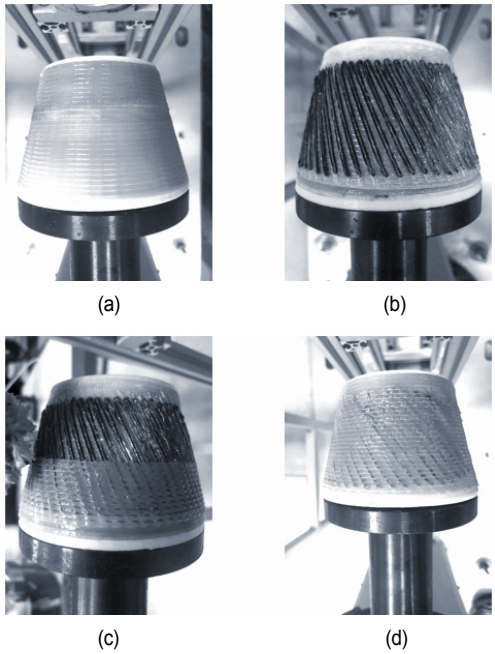

Fig. 18. The fiber placement process on the curved surface based on FDM: (a) resin layer; (b) the process of fiber placement; (c) the process of resin filling; (d) composite conical shell.

5. Production

A six-axis industrial robot and spindle were used here to produce composite cone shells. We designed a dual nozzle device that can switch nozzles. We controlled the movement of the robot and the rotation of the spindle by writing procedure codes.

At the beginning of placement, the robot and the spindle moved together and the resin was deposited on the curved surface according to the path. Then we switched the nozzles and placed the carbon fiber on the resin layer. To place the fiber continuously on the curved surface, we connected the path after the fiber was rotated, as shown in Fig. 18(b). Finally, we switched the nozzle again and covered the carbon fiber with resin. The placement condition is shown in Fig. 18. How-

ever, during the placement process, the carbon fiber at both ends was not completely cooled and was dragged back by the nozzle. This is a problem we will focus on later.

6. Conclusions

We have derived three types of fiber paths on the surface of the conical shell according to the differential geometry and designed the paths of resin filling. We used MATLAB (R2016b) to simulate the placement results, analyze the critical parameters of different paths, fiber direction angle, curvature and fiber content. The result shows that:

1) The range of parameter φ_0 of the geodesic path is 0° to 42°. The parameter ξ of the linear curve is not limited and the maximum value of the parameter C of the constant curvature curve is 0.032.

2) The direction angle of the geodesic path is between 0° and 75°. The direction angle of the linear curve hardly changes and the fiber direction of the constant curvature curve can be designed best, and the range of the direction angle is -90° to 90°.

3) The maximum curvature k_n of the geodesic path is equal to 0.027 and $\mathrm{k_g}$ is equal to 0. The maximum curvature k_n of the linear curve is 0.03 and $\mathrm{k_g}$ are all less than 0.009. As for the constant curvature curve, the maximum curvature k_n is 0.03 and $\mathrm{k_g}$ is equal to the parameter C.

4) The fiber content of the geodesic path is greatly affected by the parameter φ_0, and the difference can reach 40 %. The fiber content of the linear curve is greater than 90 %. When ξ is equal to 4, the fiber content is 95 %. The fiber content of the constant curvature curve is generally very low, about 20 %.

We used a six-axis robot and a spindle to produce composite conical shell with fibers evenly distributed on the curved surface.

In the future, we will optimize the process parameters and study new fiber path planning methods to reduce the gap between fibers. This will help increase the fiber content and improve surface quality.

Acknowledgments

Opening Foundation of Shanghai Collaborative Innovation Center for High Performance Fiber Composites (Grant No. X12812001/047) and Opening Foundation of State Key Lab of Digital Manufacturing Equipment & Technology (Grant No. DMETKF2021019), Research Project of State Key Laboratory of Mechanical System and Vibration MSV202213 support this study.

Nomenclature

r_θ : Partial derivative of surface to θ
r_z : Partial derivative of surface to z
ds : Arc length element
I : The first basic form of curved surface
II : The second basic form of curved surface
k_n : Normal curvature
k_g : Geodesic curvature

References

[1] T. M. Yu, H. B. Bing, B. M. Wang, C. H. Guo and F. C. Jiang, Research progress of molding process of fiber reinforced thermoplastic composites, *Engineering Plastics Application,* 46 (2018) 139-144.

[2] F. Van Der Klift, Y. Koga, A. Todoroki, M. Ueda, Y. Hirano and R. Matsuzaki, 3D printing of continuous carbon fibre reinforced thermo-plastic (CFRTP) tensile test specimens, *Open J. of Composite Materials*, 6 (2016) 18-27.

[3] Y. Nakagawa, K.-I. Mori and Y. Maeno, 3D printing of carbon fibre-reinforced plastic parts, *The International J. of Advanced Manufacturing Technology,* 91 (2017) 2811-2817.

[4] Y. Yamanaka, A. Todoroki, M. Ueda, Y. Hirano and R. Matsuzaki, Fiber line optimization in single ply for 3D printed composites, *Open Journal of Composite Materials,* 6 (2016) 121-131.

[5] R. Matsuzaki, M. Ueda, M. Namiki, T.-K. Jeong, H. Asahara, K. Horijuchi, T. Nakamura, A. Todoroki and Y. Hirano, Three-dimensional printing of continuous-fiber composites by in-nozzle impregnation, *Scientific Reports*, 6 (1) (2016) 23058.

[6] G. T. Mark and A. S. Gozdz, *Methods for Composite Filament Fabrication in Three Dimensional Printing*, Patent No. US9126365B1, U.S. Patents and Trademark Office (2015).

[7] R. Reese and H. Bheda, *Heated Build Platform and System for Three Dimensional Printing Methods*, Patent No. US9592660B2, U.S. Patents and Trademark Office (2016).

[8] V. Schillen and A. El-Siblani, *Process and Device for Producing a Three-dimensional Object*, Patent No. US8845316B2, U.S. Patents and Trademark Office (2014).

[9] X. Y. Tian, T. F. Liu, C. C. Yang, Q. R. Wang and D. C. Li, Interface and performance of 3D printed continuous fiber reinforced PLA composites, *Composites: Part A*, 88 (2016) 198-205.

[10] M. Lu, Fundamental research on path generation algorithm of composite components in automatic fiber placement, *Ph.D. Thesis*, Nanjing University of Aeronautics and Astronautics, China (2011).

[11] A. Tullu, T. W. Ku and B. S. Kang, Elastic deformation of fiber-reinforced multi-layered composite conical shell of variable stiffness, *Composite Structures,* 154 (2016) 634-645.

[12] Y. J. Liu, X. F. Wang and J. Jun, Trajectory planning method for constant curvature curve of cone, *Acta Aeronautics et Astronautics Sinica,* 38 (7) (2017).

[13] D. Del Rossi, V. Cadran, P. Thakur, M. Palardy-Sim, M. Lapalme and L. Lessard, Experimental investigation of the effect of half gap/half overlap defects on the strength of composite structures fabricated using automated fibre placement (AFP), *Composites Part A*, 150 (2021) 106610.

[14] W. Y. Liu, X. L. Hou, B. S. Tan, S. N. Sang and Y. B. Fan, Path planning and simulation of curved surface layering-based directional 3D printing, *J. of Machine Design*, 35 (S1) (2018)

10-14.
[15] Z. Y. Wang, J. K. Min and G. L. Xiong, Robotics-driven printing of curved 3D structures for manufacturing cardiac therapeutic devices, *IEEE International Conference on Robotics and Biomimetics* (2015) 2318-2323.
[16] Z. B. Xin, Y. G. Duan, W. Xu, T. Y. Zhang and B. Wang, Review of the mechanical performance of variable stiffness design fiber-reinforced composites, *Sci. Eng. Compos. Mater.*, 25 (3) (2018) 425-437.
[17] Z. Z. Pan, L. W. Zhang and K. M. Liew, A phase-field framework for failure modeling of variable stiffness composite laminae, *Computer Methods in Applied Mechanics and Engineering*, 388 (2022) 114192.
[18] J. F. LI, Research on automated fiber placement trajectory plan-ning method of adjustment algorithm based on structural design for surface with holes, *Master's Thesis*, Nanjing University of Aeronautics and Astronautics, China (2013).
[19] M. A. Caminero, J. M. Chacon, I. Garcia-Moreno and G. P. Rodriguez, Impact damage resistance of 3D printed continuous fiber reinforced thermoplastic composites using fused deposition modelling, *Composites Part B*, 148 (2018) 93-103.
[20] Z. D. Shan, C. Z. Fan, Q. L. Sun and L. Zhan, Research on additive manufacturing technology and equipment for fiber reinforced resin composites, *China Mechanical Engineering*, 31 (2) (2020) 221-226.

Kangmei Li is an Associate Professor and Master's Supervisor at College of Mechanical Engineering, Donghua University, Shanghai, China. Her research interests include laser precision processing, surface texturing technology, manufacturing technique of composite structures.

Jun Hu is a Professor and Doctoral Supervisor at the Institute of Artificial Intelligence, Donghua University, Shanghai, China. His research interests include CNC technology and equipment, laser fine processing technology and manufacture technique of composite structures.